The Cryosphere Discuss., 7, 1141–1176, 2013
www.the-cryosphere-discuss.net/7/1141/2013/
doi:10.5194/tcd-7-1141-2013

The Cryosphere Discussions
Open Access

Cyclone impact on sea ice in the central Arctic Ocean: a statistical study

A. Kriegsmann[1,*] **and B. Brümmer**[1]

[1]Meteorological Institute, University of Hamburg, Germany
[*]now at: Climate Service Center, Hamburg, Germany

Received: 9 January 2013 – Accepted: 25 February 2013 – Published: 21 March 2013

Correspondence to: A. Kriegsmann (arne.kriegsmann@zmaw.de)

Published by Copernicus Publications on behalf of the European Geosciences Union.

Abstract

This study investigates the impact of cyclones on the Arctic Ocean sea ice for the first time in a statistical manner. We apply the coupled ice–ocean model NAOSIM which is forced by the ECMWF analyses for the period 2006–2008. Cyclone position and radius detected in the ECMWF data are used to extract fields of wind, ice drift, and concentration from the ice–ocean model. Composite fields around the cyclone centre are calculated for different cyclone intensities, the four seasons, and different regions of the Arctic Ocean. In total about 3500 cyclone events are analyzed. In general, cyclones reduce the ice concentration on the order of a few percent increasing towards the cyclone centre. This is confirmed by independent AMSR-E satellite data. The reduction increases with cyclone intensity and is most pronounced in summer and on the Siberian side of the Arctic Ocean. For the Arctic ice cover the impact of cyclones has climatologic consequences. In winter, the cyclone-induced openings refreeze so that the ice mass is increased. In summer, the openings remain open and the ice melt is accelerated via the positive albedo feedback. Strong summer storms on the Siberian side of the Arctic Ocean may have been important reasons for the recent ice extent minima in 2007 and 2012.

1 Introduction

Arctic sea ice extent and thickness have undergone a significant decline in the last decade (Stroeve et al., 2012) with the latest record sea ice extent minimum in September 2012. The reasons are manifold and cannot be assigned to one process only. However, it is generally accepted that the decline is also a signature of anthropogenic climate change (Notz and Marotzke, 2012).

Although sea ice is finally the result of local thermodynamic freezing and melting, there are other processes that significantly influence the sea ice formation. In addition to radiation, temperature advection and others, the dynamic impact of cyclones has substantial impacts on the sea ice cover. The strong, inhomogeneous wind field deforms the ice cover and causes cracks, leads and polynias. The thermodynamic effect of these openings is different in winter and summer. In winter, the openings are the places with the largest heat fluxes from the ocean to the atmosphere. The openings refreeze so that the heat fluxes decrease with time and salt is released from the newly formed ice to the ocean. In summer, refreezing does not occur, so that almost all downwelling shortwave radiation is absorbed. This leads to a local warming of the uppermost ocean layer and promotes further ice melt.

The potential of cyclones to significantly affect the sea ice has been demonstrated in many case studies. Zwally and Walsh (1987) investigated by means of satellite images and model data the local change in ice concentration under the influence of a wintertime cyclone north of Alaska. Even though the impact of the wind field of the cyclone lasted only between one and three days, the reduction of the multiyear sea ice persisted for months, as can been seen in the satellite images.

With satellite data and ice drift buoy measurements Maslanik and Barry (1989) found for wintertime situations in the Canadian part of the central Arctic, that cyclones lead to reductions in sea ice concentration and increased divergence of the sea ice drift. Barry and Maslanik (1989) also report a reduction in sea ice concentration in summer in the Canadian part of the Arctic, caused by cyclonic conditions in the wind field and the associated divergent and sheared ice drift.

In the western Arctic, a strong cyclone reduced the sea ice concentration by 3 to 5 % in October 1991 (Maslanik et al., 1995). A measured increase in the fraction of first year ice was attributed to the freezing of the cyclone induced open water areas.

Through the breaking of the ice cover, internal stress within the ice is reduced and the mobility of the ice floes is increased. The ratio of ice drift speed and wind speed (the wind factor) is increased for a short time after the cyclone passage (Brümmer and Hoeber, 1999).

On the basis of satellite images, Holt and Martin (2001) investigated the passage of a cyclone through the Beaufort Sea, the Chukchi Sea, and the East Siberian Sea in

TCD
7, 1141–1176, 2013

Cyclone impact on sea ice in the central Arctic Ocean

A. Kriegsmann and B. Brümmer

August 1992. They report a growth of the fraction with open water and a decrease in the size of floes.

Brümmer et al. (2003) also found on the basis of buoy measurements cyclone induced inertial oscillations or tidal oscillations in the Fram Strait. They show, that the oscillations are also detectable in the divergence, the vorticity and the deformation of the ice drift. An ice drift, that is convergent in the cyclone center and divergent on the outside, was observed for a cyclone on 13 and 14 March 2002 (Brümmer et al., 2008).

Lammert et al. (2009) also report a cyclone that reduced the sea ice concentration by 11 % and induced inertial oscillations in the sea ice in the Fram Strait on 23 March 2007.

Screen et al. (2011) investigate the relationship between sea ice extent at the end of the Arctic summer, and cyclone activity in the preceding spring and summer. They find that fewer cyclones over the central Arctic Ocean in May, June, and July favour a low sea ice extent at the end of the melt season.

In this paper, we use a statistical approach to quantify the local impact of cyclones on the sea ice in the Arctic Ocean, using a combination of observations and modelling. We use the six-hourly analyses of the ECMWF (European Centre for Medium-Range Weather Forecasts) as atmospheric forcing of the coupled ice–ocean model NAOSIM (*N*orth Atlantic *A*rctic *O*cean *S*ea *I*ce *M*odel). Within an area with a certain radius around the detected cyclone position the model-simulated impact on the sea ice is determined with respect to ice concentration and the wind-ice drift relation. The model results for the individual cyclone cases are composed for different classes. These are: different cyclone intensities, different seasons, and different sub-areas of the Arctic Ocean. For all classes, the spatial distribution of wind, drift, and concentration within the cyclone radius and the time evolution from before, during, to after the cyclone event is investigated. The study is based on a three-year period 2006–2008.

The paper is organized as follows: Sect. 2 describes the model and Sect. 3 the methods of cyclone detection and the study area. The results of the statistical analyses of the impact of the cyclones on sea ice in the central Arctic Ocean is presented in

Sect. 4 with respect to the cyclone intensity, to seasonal differences, and to regional differences. Finally, the conclusions are presented in Sect. 5.

2 The ice–ocean model

The model NAOSIM is a coupled sea ice–ocean model. The ocean part is based on the Modular Ocean Model 2 of the Geophysical Fluid Dynamics Laboratory. The sea ice part is the dynamic-thermodynamic ice model based on the work of Hibler (1979), and was enhanced, for example, in the subgrid sea ice thickness (Hibler, 1984) and in the rheology (Harder, 1996). The sea ice follows a viscous-plastic rheology. The prognostic variables of the ice model are sea ice concentration and thickness, snow height, and sea ice drift. The model domain covers the whole Arctic and the North Atlantic with a southern border at 50° N. The x-axis is parallel to the 30° W/150° E longitude line. The spatial resolution is ≈ 9 km. The model needs a prescribed atmosphere every 6 h. In this work, forcing data of the ECMWF analysis are used. These data have a spatial resolution of 25 km and are interpolated to the 9 km model grid. The forcing variables are temperature, dewpoint temperature, wind, wind stress, cloud cover, and precipitation. The latter is taken from ECMWF 6 h-forecast.

The quality of the simulated ice drift increases with the distance from the coast (not shown). Thorndike and Colony (1982) showed that the impact of the coast on the ice drift is detectable up to a distance of 400 km. Therefore, we restrict our studies to those parts of the Arctic Ocean that are at least 300 km distant from the next coast. Between 0° E and 45° E, the 85. degree of latitude was chosen as border so that the Fram Strait is not included in the study area (Fig. 1).

3 Cyclone detection

Cyclone position, radius, and intensity are determined from the 6-hourly sea level pressure field of the ECMWF analysis for the period 2006–2008 applying the algorithm of

Murray and Simmonds (1991). In the beginning, the first and the second derivatives of the two-dimensional sea level pressure p are calculated at all grid points. Grid points, where the Laplace operator $\nabla^2 p = p_{xx} + p_{yy}$ which is proportional to the geostrophic vorticity has a local maximum and is above a certain threshold, are candidates for a cyclone. In the case that a pressure minimum in the surrounding of this point exists, the exact position of the cyclone core is calculated. The cyclone detection according to Murray and Simmonds (1991) depends on many settings, for example on the threshold of $\nabla^2 p$, on the search radius around the maximum of the Laplace operator, on the search area and the kind of search. For cyclone tracking, the detections are connected to cyclone tracks, based on probability calculations regarding cyclone track direction, cyclone speed, and core pressure among others.

In this work, in addition to position and time of a detection two further quantities are used: the radius and the intensity of a cyclone. The radius is defined as a weighted distance between core and margin of a cyclone, where margin is the place with $\nabla^2 p = 0$. The intensity of a cyclone is defined as $\nabla^2 p$.

The cyclone dataset which we use is that which was prepared by Haller (2011), and contains all detections for the area north of 60° N, for the period 2006–2008. This amounts to a total of 70 405 detections belonging to 7987 cyclones (Table 1). On average, each cyclone has 5.05 detections, i.e. a lifetime of about 30 h.

The automated detection of cyclones is an often applied method. For example, Jahnke-Bornemann (2010) uses an automated procedure of Blender et al. (1997) for investigations of cyclones in the Norwegian Sea. Also with an automatical procedure, Serreze and Barrett (2008) found in reanalyses of the National Centers for Environmental Prediction (NCEP) in the long-time mean a maximum of cyclones in the central Arctic during the summer. Affeld (2003) used automatically detected cyclones to investigate the impact of cyclones on the ice transport through the Fram Strait. A good review of the different approaches to detect (and track) cyclones is given in Ulbrich et al. (2009).

On the basis of the position of the cyclones the mean impact on ice concentration and ice drift was investigated. The cyclone detections were sorted into different classes in order to find out how the impact of the cyclone in the sea ice varies with the cyclone intensity, the seasons, and the different Arctic regions.

In order to compare the model-simulated changes in ice concentration with observed changes we use the satellite-based AMSR-E microwave (89 GHz) ice concentration. The AMSR-E ice concentration data have a horizontal resolution of 6.5 km and a time resolution of one day. For the comparison, the AMSR-E data are interpolated to the 9 km model grid. Sometimes the ice-covered area in the simulation and from the AMSR-E data do not match well. This is mainly the case in summer (Fig. 2) when AMSR-E has the tendency to overestimate the ice concentration (Spreen et al., 2008). Therefore, all detections with a difference in the mean ice concentration within the cyclone radius of more than 10 % are neglected for the cyclone impact study (called ADiff-Filter). This ADiff-filter removes about 30 % of the detections (Table 1).

4 Statistical analysis of the impact of cyclones on the sea ice

In this section the impact of cyclones on the Arctic Ocean sea ice is presented and distinguished with respect to three impact categories. The first category is the strength of the atmospheric forcing which we assume to be represented by the cyclone intensity. The second category is the season because in addition to, e.g. different air temperatures a cyclone meets different sea ice conditions such as concentration, thickness, or ice strength and, thus, the consequences on the different sea ice are expected to be different. The third category is the sub-region of the Arctic Ocean because the sea ice has a distinct gradient, e.g. in thickness from the Siberian (thin) to the Canadian side (thick) and belongs to different drift regimes (Transpolar Drift, Beaufort Gyre).

Each impact category (intensity, season, region) is subdivided into four classes. For each class composite fields for wind, ice drift and concentration around the cyclone are calculated. This is performed in a relative horizontal coordinate frame which is normalized with the cyclone radius. The composite averaging is made without any rotation of the frame (e.g. with respect to North). So, the relative x, y frame in the figures below is parallel to the axes of the model domain (see Sect. 2).

4.1 Cyclone intensity

The intensity $I = \nabla^2 p$ of all cyclone detections in the study area during the period 2006–2008 ranges from $I = 0$ to $I = I_{max}$ (= 6.72 hPa latitude^{-2}). We distinguish between four intensity classes belonging to the four quartiles of the frequency distribution. The intensity range for each class together with the average cyclone radius is given in Table 2.

For each class the mean wind vector field and the mean wind speed are shown in Fig. 3 (top). The cyclonic structure of the wind field is not limited to the detection radius, but reaches twice the detection radius. As expected, with increasing intensity also the wind speed increases. The maximum mean wind speed increases from about 4 m s^{-1} in I_1 to almost 9.5 m s^{-1} in I_4. The wind speed slows down towards the cyclone center where it is around 2.5 m s^{-1} in I_1 and 4.5 m s^{-1} in I_4.

The wind fields in Fig. 3 are not rotationally symmetric but show the highest winds and, thus, the strongest pressure gradients in the direction towards the negative x- and y-directions. This is (see Fig. 1) the direction from the North Atlantic side to the Pacific side of the Arctic Ocean, and coincides with the gradient of the climatologically mean sea-level pressure distribution which exhibits lower pressure over the Northeast Atlantic and higher pressure over the East-Siberian Sea and Beaufort Sea (Serreze and Barry, 2005). If a symmetric cyclone pressure field is superposed to this climatologic pressure distribution the resulting pressure gradient in the cyclone is stronger on the side towards the climatologic high pressure than towards the low pressure.

The mean ice drift field in Fig. 3 (bottom) clearly has the same cyclonic structure as the wind field. This is true for all intensity classes. Inside the radius in accordance with decreasing wind, ice drift decreases.

In the Northern Hemisphere, the Coriolis force causes a rotation of the ice drift to the right in relation to the wind. The angle between wind and ice drift depends on the intensity of the cyclone only to a minor degree (Fig. 4 top). The angle is between 30° and 35° for most of the cyclone-influenced area, but decreases to significantly smaller values in the vicinity of the cyclone center. The spatial distribution of the wind factor (speed of ice drift versus wind speed) in Fig. 4 (bottom) shows that the wind factor increases with increasing intensity.

The reason, why the wind factor increases with increasing wind, is the following: Wind stress $\boldsymbol{\tau}_\mathrm{a}$ is the main reason for the acceleration of ice, and is calculated as

$$\boldsymbol{\tau}_\mathrm{a} = \rho_\mathrm{a} c_\mathrm{a} |\boldsymbol{u}_{10\,\mathrm{m}}| \boldsymbol{u}_{10\,\mathrm{m}}, \tag{1}$$

where ρ_a is the density of air, c_a is the atmospheric drag coefficient and $\boldsymbol{u}_{10\,\mathrm{m}}$ the 10 m-wind. Since the drift follows the wind stress and the wind stress is proportional to the square of wind speed $\boldsymbol{u}_{10\,\mathrm{m}}$, the wind factor $u_i/\boldsymbol{u}_{10\,\mathrm{m}}$ should be linearly dependent on $\boldsymbol{u}_{10\,\mathrm{m}}$.

This is confirmed, for example, by Perrie and Hu (1997); they simulate the trajectories of ice floes with an ice sheet model. Under the assumption, that the internal forces are negligible, they found a wind factor of 2.3 % with a 10 m-wind of 10 m s^{-1} and of 4 % with a 10 m-wind of 18 m s^{-1}. For thin ice (0.5 m), Omstedt et al. (1996) calculated an increase of the wind factor with an increase of wind speed from 7 to 25 m s^{-1}. However, the increase was only from 2.3 % to 2.7 %. They neglected internal forces, too. Furthermore, the figure shows, that an area with high wind factor in the cyclone core appears only when the intensity is low. The reason may be, that the wind speed in this case is low, so that the ocean current is more important for the ice drift. The ocean current does not let the ice come to rest when the wind is zero, so that the ratio drift/wind, i.e. wind factor, becomes larger.

How do wind, drift, and wind factor develop over time during a cyclone passage? To answer this we calculate the composite fields not only for the time of cyclone detection but also for all time steps from two days before to five days after the cyclone passage, all in the same area where the cyclone was detected. In a second step, the mean of the mean field (wind, ice drift etc.) within the radius is calculated. The results are shown in

TCD
7, 1141–1176, 2013

Fig. 5. The wind factor is not the ratio of mean ice drift and mean wind but is the mean of the individual ratios (at each grid point and time step). The ratio ice drift/wind can be arbitrarily high for small wind speed, therefore the wind factor was only taken into account when the wind stress was at least 0.01 $\mathrm{N\,m^{-2}}$, that corresponds according to Eq. (1) to a wind of at least 1.76 $\mathrm{m\,s^{-1}}$.

For I_4, the time series of the wind speed shows a development over time that is different to that of the other intensity classes: in I_4, the wind has its distinct maximum around t_0, whereas in I_1, I_2 and I_3 the wind speed has a minimum to that time.

The different behaviour is due to the wind speed in Fig. 3. In I_1 and I_2 the wind speed is highest at the margin of the single radius, to the core it decreases, and outside the radius the wind speed is relatively constant. If the wind field of such a cyclone approaches the place of detection, it becames clear, that the mean wind speed within the single radius decreases the nearer the cyclone is, and that it becomes minimal at the time of detection, because than the wind field is centered over the area used for the calculation. In I_4, the situation is different: there, the maximum of the wind speed is outside the single and inside the double radius. That means, with the approach of the cyclone to the place of detection, the wind within the single radius at the place of detection has to increase, because one side of the cyclone with its maximum wind speed crosses the area within the single radius. I_3 is a transition class between the other classes.

Averaging over the whole 7-days period, the wind speed increases with the intensity. As expected, the time series of the ice drift are similar to the time series of the wind speed. The time series of the wind factor are different for the intensity classes: in I_1, I_2, and I_3 the mean wind factor decreases until the time of detection, whereas in I_4, it reaches its maximum at the time of detection.

In the following, the changes in ice concentration are investigated: for all detections of an intensity class the change in ice concentration within 24 h is calculated and then the mean change over the 24 h period is calculated (Fig. 6).

TCD
7, 1141–1176, 2013

In all intensity classes a reduction in ice concentration around the core is simulated. With increasing intensity, the area, where ice concentration is reduced, becomes larger, and the reduction becomes stronger. The change at the position of the core is at $-0.65\,\%\,\mathrm{day}^{-1}$ in I_1 and at $-2.11\,\%\,\mathrm{day}^{-1}$ in I_4. The 24 h ice concentration change based on AMSR-E is also shown in Fig. 6. It should be kept in mind that the time resolution of the AMSR-E fields is one day and that a field is composed from several satellite orbits. For the calculation of the ice concentration change, we assume that the daily fields hold for 12 UTC and then interpolate the daily fields to the time of cyclone detection ($t = 0$) and to $t = 24$ h. The 24 h change in the AMSR-E sea ice concentration shows no major difference between the I_1 to I_3. The ice concentration decreases in the core of the cyclone by up to $-1\,\%\,\mathrm{day}^{-1}$. The single radius area is surrounded by an area with ice concentration increase. In I_4, the reduction in sea ice concentration is stronger than in the other three classes. Altogether, AMSR-E observations confirm that the ice concentration is reduced within the radius of the detection and that the ice reduction increases with increasing cyclone intensity.

4.2 Seasonal differences of cyclone impact

The number of detections in the study area during the period 2006 to 2008 is almost the same in all seasons. However, due to the problem of incorrect AMSR-E ice concentration data we had to reduce the number of available detections in summer and autumn to those cases where simulated and observed ice concentration are in the same range (Table 2). The reason is the problem of correct determination of ice concentration from the microwave signal in summer.

The composite wind fields for winter (DJF), spring (MAM), summer (JJA), and autumn (SON) are presented in Fig. 7. As for the intensity classes, the cyclonic wind field is not rotationally symmetric for the above-mentioned reasons. On average, the wind is weaker in summer than in autumn and winter. However, the differences are not large: the maximum is $6.2\,\mathrm{m\,s}^{-1}$ in summer and $6.8\,\mathrm{m\,s}^{-1}$ in winter. This reflects the fact that the frequency distribution of cyclone intensities is not much different between the seasons as can be seen in Fig. 8. The cyclone activity in the central Arctic is also high in summer. The summertime maximum of cyclone detections is placed over the central Arctic Ocean (Serreze and Barrett, 2008). The ice-drift fields (not shown) exhibit an analogous pattern to the wind pattern and have the same ranking of the seasons concerning drift speed.

Figure 9 (top) shows the mean angle between 10 m-wind and ice drift for the different seasons. The angle difference is first calculated for the individual cyclone detections and then averaged. In autumn and winter, the angle is between 25° and 35° outside of the cyclone core region, in spring between 25° and 40° and in summer between 35° and 45°. As it was already found in the studies about the cyclone intensity, around the core of the cyclones there is an area with very small angles. The results of the simulation are in close agreement with Thorndike and Colony (1982). For the Arctic, they found angles in reference to the geostrophic wind of 5° in winter and spring, of 18° in summer, and of 6° for autumn. The angle between geostrophic wind and 10 m-wind is 30° in winter and 24° in summer, resulting in angles between 10 m-wind and ice drift of 35° in winter and 42° in summer.

The wind factor is around 2 % in general (Fig. 9 bottom). Averaged over the area within the cyclone radius, the wind factor is small in winter (median 2.00) and spring (median 1.93). It becomes larger in summer (median 2.02) and is largest in autumn (median 2.12). The latter appears to be a consequence of the higher wind speed and the not yet compact ice cover in SON. On average, the wind factor shows a pattern within the cyclone area in all seasons with decreasing values towards the positive x-direction and negative y-direction. This is the direction towards the Canadian side of the Arctic Ocean (see Fig. 1) where the thickest sea ice occurs and, thus, the internal ice stress is large.

The general impact of cyclones on sea ice concentration consists of a 24 h-reduction within the radius of the cyclone in all seasons (Fig. 10). The reduction is most pronounced in spring and summer.

In the core of the cyclone the ice concentration is reduced within 24 h by 0.92 % in winter, 1.67 % in spring, 2.53 % in summer and 1.17 % in autumn.

For a closer investigation of the cyclone-induced part of the ice concentration changes the annual cycle of sea ice concentration has to be considered. Ice melting in summer and freezing in winter result in a long-term (longer than the cyclone event) decrease and increase of the sea ice concentration, respectively. These trends superimpose the cyclone impact on the ice concentration. This effect can be seen in Fig. 10. The outer area (beyond 1.5 times the detection radius) shows no change in ice concentration in winter, a slight decrease in spring, a stronger decrease in summer, and an increase in autumn. For comparison, the 24 h change in the observed AMRS-E ice concentration is shown in Fig. 10. The significant features from the simulations are also present in the satellite observations: cyclones reduce the sea ice concentration in all seasons. Outside the cyclone radius the mean seasonal trends of ice concentration are present: constant in winter, variable (decrease as well as increase) in spring, decrease in summer, and increase in autumn.

Figure 11 shows the temporal evolution of ice concentration within the cyclone radius in comparison to the ice concentration trend in the whole study area. In winter, temperatures are far below the freezing point and the ice concentration is high ($> 97\,\%$). Open water, caused by cyclones, freezes quickly and the ice concentration recovers ~ 5 days after the passage of the cyclone. In spring the mean ice concentration is around 97 %. However, areas of open water, caused by cyclones, do not freeze as quickly as in winter. They exist even after a few days. The reason is the onset of the warming due to the solar radiation. In summer the ice concentration is around 77 % and is reduced by 2 % per week even without cyclone impact. However, with cyclones the reduction is accelerated to 4 % per week. In autumn the mean ice concentration is about 83.5 % and new ice is formed in large areas of the region. The sea ice concentration in the whole study area increases by around 2.5 % per week. Under the influence of a cylone, the sea ice concentration growths only by 1.5 % per week, resulting in a sea ice concentration of 85 % after a week. An important difference between the seasons is that the

TCD
7, 1141–1176, 2013

A. Kriegsmann and B. Brümmer

impact of a cyclone in winter is nearly completely vanished after 5 days, whereas in the other seasons the impact is clearly visible. In summer the difference between mean ice concentration in the whole study area and mean ice concentration within the area of detection is 2 % even after five days. The change in ice concentration relative to the time of detection highlights the quantitatively stronger reduction in summer (Fig. 11 bottom).

The seasonal difference in the duration of a cyclone's impact can have extensive climatological consequences. A lot of studies were done on the change of cyclone activities. Some of them found an increase of the number of cyclones in the Arctic (e.g. Sepp and Jaagus, 2011). Zhang et al. (2004) found, that the number of summer cyclones increases. If the number of cyclones in the summer increases, than the melting of sea ice can be accelerated.

4.3 Cyclone impact in different regions of the Arctic Ocean

We sub-divide the study area into four regions: Siberian sector (Sib), Canadian sector (Can), North Pole region on the Siberian side (NP-S), and North Pole region on the Canadian side (NP-C) (Fig. 1). The regions were chosen in a way that all have about the same numbers of detections (Table 2) and that the ice conditions differ. For example, in the Can sector often thick ice is found moving with the Beaufort Gyre. The sea ice in the Sib sector is thinner and moves with the Transpolar Drift towards the Fram Strait.

The mean wind speed is highest in NP-S which is closest to the North Atlantic low-pressure zone, followed by Sib, NP-C, and Can which is close to the Arctic high pressure zone. Mean ice drift follows the same ranking (not shown).

The wind factor is highest in Sib where the thinnest ice is present, followed by NP-S, NP-C, and Can where the thickest ice is present (Fig. 12). Sectors Sib and NP-S are rather similar and so are the sectors Can and NP-C. For NP-C and Can, there are relatively more grid-points within the cyclone radius with a small wind factor below 1.75 %. This is attributed to the thick and compact ice that piles up ahead the Canadian coast and that drifts relatively slow. In single cases, when the cyclone is at the margin of the study area and when the radius is large enough, the ice along the Canadian coast is part of the calculation of the wind factor.

In all regions, the mean wind within the cyclone radius increases when the time of detection and, thus, the cyclone approaches (Fig. 13 top). At the time of detection ($t = 0$) the wind speed decreases. Wind speeds in the regions Can and NP-C are nearly identical and are the smallest, compared to the other regions. Wind speed in the Sib sector is slightly higher. In these three regions, the wind speed varies similarly with time, whereas in NP-S not only the wind speed is highest, but also the wind extremes occur at other times and the minimum is less distinct.

The mean ice drift during a cyclone event is slowest in the Can and NP-C regions. The fastest moving ice can be found in NP-S, where the wind is strongest.

The time variation of the wind factor during the cyclone passage shows different behaviour: in Sib and NP-S, the passage is connected with an increase of the wind factor of 0.05 % resp. 0.1 %. In contrast to that, in NP-C and Can the wind factor decreases by about 0.75 % resp. 0.2 %. Again, the reason for this is the thick and compact ice towards the Canadian coast.

The change of ice concentration within 24 h after detection is similar in all regions. The reduction is between 1.12 % in NP-S and 1.67 % in Can (not shown). The time series of ice concentration within the cyclone radius show that the mean ice concentration two days before the detection starts at different levels between 91.5 % in Sib and 97 % in NP-C (Fig. 14 top). In all regions, the ice concentration five days after detection is reduced, compared to the mean ice concentration in the whole study area, and below the value it had before the cyclone passage. Relating the ice concentration to that at the time of detection (Fig. 14 bottom), there is a similar development of the ice concentration in NP-C, Can, Sib regions. The reduction is largest with 1.8 % in Can.

TCD
7, 1141–1176, 2013

5 Conclusions

In this study the impact of cyclones on the sea ice in the central Arctic Ocean was investigated, in contrast to many case studies, for the first time in a statistical manner. To this end we applied the coupled ice–ocean model NAOSIM and forced it with the 6-hourly ECMWF analysis data for the period 2006–2008. Cyclone position and radius detected from the ECMWF sea-level pressure were used to extract the local fields of wind, ice drift, and concentration within twice the cyclone radius for a time interval from 2 days before to 5 days after the cyclone passage. The cyclone impact is quantified by the drift-wind speed ratio and angle difference and the change of ice concentration. Centred at the cyclone position and normalized by the cyclone radius, composite fields of these quantities are calculated for different cyclone intensities, the four seasons, and different regions of the Arctic Ocean.

The classification of the cyclones according to their intensities shows that wind speed, ice drift, and wind factor increase with increasing intensity. In contrast to that, the angle difference between 10 m-wind and ice drift does not depend on the intensity. In general, the cyclone passage leads to a reduction of the ice concentration which increases from the cyclone edge to the centre. In the centre, the reduction within 24 h after the passage is on the order of 0.5 to 2 % increasing with cyclone intensity. This spatial distribution and ranking of the ice concentration change is supported by independent AMSR-E satellite data.

Mean wind speed and ice drift within the cyclone radius show only small seasonal differences with a minimum in summer and a maximum in autumn/winter. The angle difference between 10 m-wind and ice drift is largest in summer with up to 42° and smallest in autumn/winter with up to 34°. The wind factor has a minimum in spring and a maximum in autumn. Reductions in sea ice concentration occur in all seasons, but are of different magnitude and duration. The largest reduction of up to 4 % occurs in summer and is persistent. In winter, the sea ice concentration returns to its initial value

TCD
7, 1141–1176, 2013

a few days after the passage of a cylone, which means that areas with open water refreeze quickly.

The regional investigation of cyclone impact reveals that wind speed and ice drift are strongest in the NP-S region, which is close to the North Atlantic low pressure zone, and are weakest in the Can region, which is close to the high pressure zone over the western Arctic Ocean. The wind factor is smallest in the Can region with 1.84 % and largest in the Sib region with 2.21 %. The main reason for the regional differences of cyclone impact is the different ice thickness in these sectors. The change in the wind factor due to the cyclone lasts a few days. Whether the wind factor is increased or reduced depends on the sector.

On the short time scale of a passing cyclone, freezing and melting play a minor role in the change of ice concentration. Thus, the cyclone-induced reduction of ice concentration is almost solely due to ice sheet deformation. This means that there is no loss of ice mass but that the ice is ridged. Thus, the cyclone causes more thick ice. The following processes, freezing and melting, have different longer-term or even climatologic consequences in winter and summer. In winter, the heat flux between ocean and atmosphere over the cyclone-induced open water areas is increased for a few days. This heats and moistens the shallow Arctic boundary layer. At the same time the freezing of the open water areas leads to the formation of new sea ice, so that a further important impact of the wintertime cyclones is an increase of the Arctic ice mass. In summer, the cyclone-induced reduction of sea ice concentration is largest and the open water areas remain open. This summertime impact is expected to be especially large in areas with thinner ice as, e.g. on the Siberian side and in the marginal ice areas of the Arctic Ocean. Strong summer storms in those areas can lead to increased exceptional reduction of the sea ice concentration. The strong summer cyclone between 4 and 8 August 2012 is believed to be one reason for the following record ice extent minimum in September 2012 (e.g. Beitsch, 2012).

Acknowledgements. This work has received support from the European Union through the 6th framework programme DAMOCLES. Work was supported in parts through the Cluster of Excellence "CliSAP" (EXC177), University of Hamburg, funded through the German Science Foundation (DFG).

References

Affeld, B.: Zyklonen in der Arktis und ihre Bedeutung für den Eistransport durch die Framstraße, PhD thesis, Meteorologisches Institut, Universität Hamburg, 2003. 1146

Barry, R. G. and Maslanik, J.: Arctic sea ice characteristics and associated atmosphere–ice interactions in summer inferred from SMMR sata and drifting buoys: 1979–1984, GeoJournal, 18, 35–44, 1989. 1143

Beitsch, A.: Sturm in der Arktis, available at: http://www.scilogs.de/wblogs/blog/klimalounge/klimadaten/2012-08-10/sturm-in-der-arktis, 2012. 1157

Blender, R., Fraedrich, K., and Lunkeit, F.: Identification of cyclone-track regimes in the North Atlantic, Q. J. Roy. Meteorol. Soc., 123, 727–741, 1997. 1146

Brümmer, B. and Hoeber, H.: A mesoscale cyclone over the Fram Strait and its effects on sea ice, J. Geophys. Res., 104, 19085–19098, 1999. 1143

Brümmer, B., Müller, G., and Hoeber, H.: A Fram Strait cyclone: properties and impact on ice drift as measured by aircraft and buoys, J. Geophys. Res., 108, 4217, doi:10.1029/2002JD002638, 2003. 1144

Brümmer, B., Schröder, D., Müller, G., Spreen, G., Jahnke-Bornemann, A., and Launiainen, J.: Impact of a Fram Strait cyclone on ice edge, drift, divergence, and concentration: possibilities and limits of an observational analysis, J. Geophys. Res., 113, C12003, doi:10.1029/2007JC004149, 2008. 1144

Haller, M.: Arktische Zyklonen und Meereisdrift während der DAMOCLES-Bojenexperimente 2007–2010, PhD thesis, Meteorologisches Institut, Universität Hamburg, 212 pp., 2011. 1146

Harder, M.: Dynamik, Rauhigkeit und Alter des Meereises in der Arktis – numerische Untersuchungen mit einem großskaligen Modell (Dynamics, roughness, and age of Arctic sea ice – numerical investigations with a large-scale model), PhD thesis, Berichte zur Polarforschung (Reports on polar research), 203, Univ., Bremen, 129 pp., 1996. 1145

Hibler III, W.: A dynamic thermodynamic sea ice model, J. Phys. Oceanogr., 9, 815–846, 1979. 1145

Hibler III, W.: The role of sea ice dynamics in modeling CO_2 increases, climate processes and climate sensitivity, Geophys. Monogr., 29, 238–253, 1984. 1145

Holt, B. and Martin, S.: The effect of a storm on the 1992 summer sea ice cover of the Beaufort, Chukchi, and East Siberian Seas, J. Geophys. Res., 106, 1017–1032, 2001. 1143

Jahnke-Bornemann, A.: Zyklonen im Europäischen Nordmeer und Zusammenhänge mit der nordatlantischen Tiefdruckrinne, PhD thesis, Meteorologisches Institut, Universität Hamburg, 2010. 1146

Lammert, A., Brümmer, B., and Kaleschke, L.: Observation of cyclone-induced inertial sea-ice oscillation in Fram Strait, Geophys. Res. Lett., 36, L10503, doi:10.1029/2009GL037197, 2009. 1144

Maslanik, J. A. and Barry, R.: Short-term interactions between atmospheric synoptic conditions and sea-ice behaviour in the Arctic, Ann. Glaciol., 12, 113–117, 1989. 1143

Maslanik, J. A., Fowler, C., Heinrichs, J., Barry, R., and Emery, W. J.: Remotely-sensed and simulated variability of Arctic sea-ice concentrations in response to atmospheric synoptic systems, Int. J. Remote Sens., 16, 3325–3342, 1995. 1143

Murray, R. J. and Simmonds, I.: A numerical scheme for tracking cyclone centers from digital data. Part I: Development and operation of the scheme, Aust. Meteor. Mag., 39, 155–166, 1991. 1146

Notz, D. and Marotzke, J.: Observations reveal external driver for Arctic sea-ice retreat, Geophys. Res. Lett., 39, L08502, doi:10.1029/2012GL051094, 2012. 1142

Omstedt, A., Nyberg, L., and Leppäranta, M.: On the ice-ocean response to wind forcing, Tellus A, 48, 593–606, doi:10.1034/j.1600-0870.1996.t01-3-00008.x, 1996. 1149

Perrie, W. and Hu, Y.: Air-ice-ocean momentum exchange. Part II: Ice drift, J. Phys. Oceanogr., 27, 1976–1996, 1997. 1149

Screen, J. A., Simmonds, I., and Keay, K.: Dramatic interannual changes of perennial Arctic sea ice linked to abnormal summer storm activity, J. Geophys. Res.-Atmos., 116, D15105, doi:10.1029/2011JD015847, 2011. 1144

Sepp, M. and Jaagus, J.: Changes in the activity and tracks of Arctic cyclones, Climatic Change, 105, 577–595, 2011. 1154

Serreze, M. and Barry, R. G.: The Arctic Climate System, Cambridge University Press, 385 pp., 2005. 1148

Serreze, M. C. and Barrett, A. P.: The summer cyclone maximum over the central Arctic Ocean, J. Climate, 21, 1048–1065, 2008. 1146, 1152

Spreen, G., Kaleschke, L., and Heygster, G.: Sea ice remote sensing using AMSR-E 89-GHz channels, J. Geophys. Res., 113, C02S03, doi:10.1029/2005JC003384, 2008. 1147

Stroeve, J. C., Kattsov, V., Barrett, A., Serreze, M., Pavlova, T., Holland, M., and Meier, W. N.: Trends in Arctic sea ice extent from CMIP5, CMIP3 and observations, Geophys. Res. Lett., 39, L16502, doi:10.1029/2012GL052676, 2012. 1142

Thorndike, A. and Colony, R.: Sea ice motion in response to geostrophic winds, J. Geophys. Res., 87, 5845–5852, 1982. 1145, 1152

Ulbrich, U., Leckebusch, G., and Pinto, J.: Extra-tropical cyclones in the present and future climate: a review, Theor. Appl. Climatol., 96, 117–131, 2009. 1146

Zhang, X., Walsh, J., Zhang, J., Bhatt, U., and Ikeda, M.: Climatology and interannual variability of arctic cyclone activity: 1948–2002, J. Climate, 17, 2300–2317, 2004. 1154

Zwally, H. J. and Walsh, J. E.: Comparison of observed and modeled ice motion in the Arctic Ocean, Ann. Glaciol., 9, 136–144, 1987. 1143

Table 1. Number of detections (cyclones).

	North of 60° N	Within study area	After ADiff-filter
2006	23 220 (2627)	1874 (316)	1245 (248)
2007	23 171 (2570)	1462 (248)	1100 (204)
2008	24 014 (2790)	1721 (304)	1151 (240)
total	70 405 (7987)	5057 (868)	3496 (692)

TCD
7, 1141–1176, 2013

Table 2. Number of cyclone detections for intensity quartiles, seasons, and regions.

intensity (% of I_{max})	no.	radius [km]	season	no.	radius [km]	region	no.	radius [km]
I_1 (0–14.7)	873	266	winter	1360	315	np-s	782	298
I_2 (14.7–20.3)	875	306	spring	1067	320	np-c	844	309
I_3 (20.3–29.0)	874	327	summer	374	303	sib	789	316
I_4 (29.0–100)	874	344	autumn	694	293	can	1080	318

TCD
7, 1141–1176, 2013

Cyclone impact on sea ice in the central Arctic Ocean

A. Kriegsmann and B. Brümmer

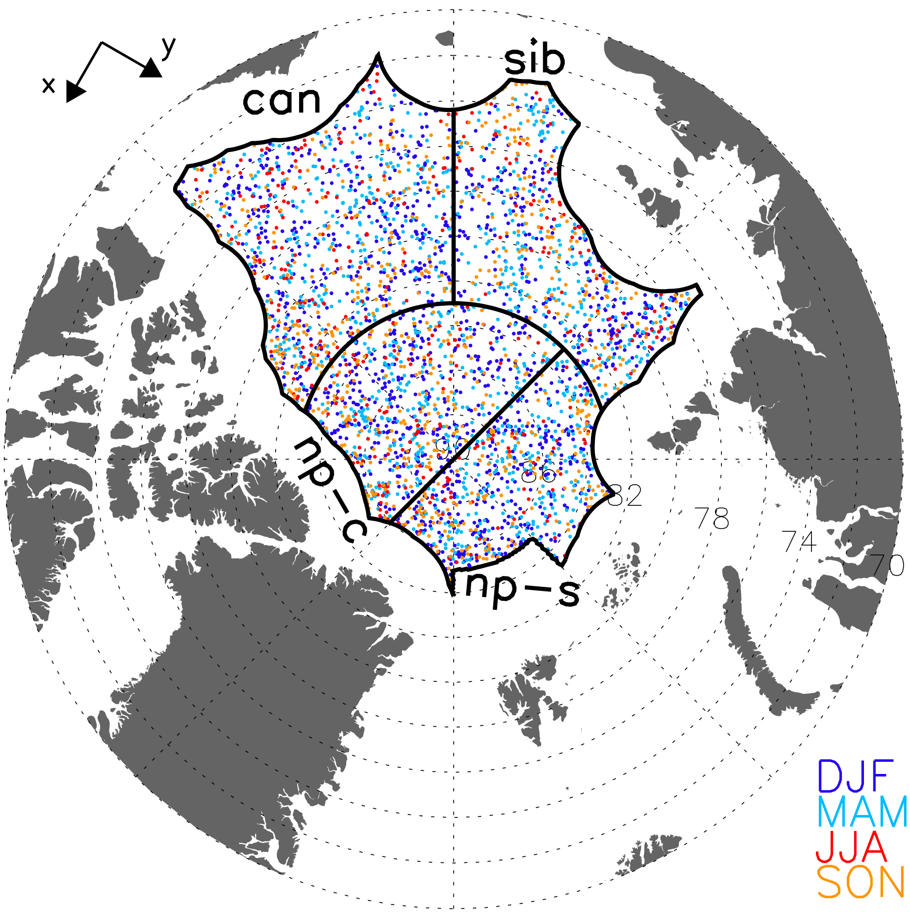

Fig. 1. Study area and spatial and seasonal distribution of the cyclone detections (dots) for the period 2006–2008. The orientation of the (x,y)-coord. axes is shown in the upper left corner.

TCD
7, 1141–1176, 2013

Cyclone impact on sea ice in the central Arctic Ocean

A. Kriegsmann and B. Brümmer

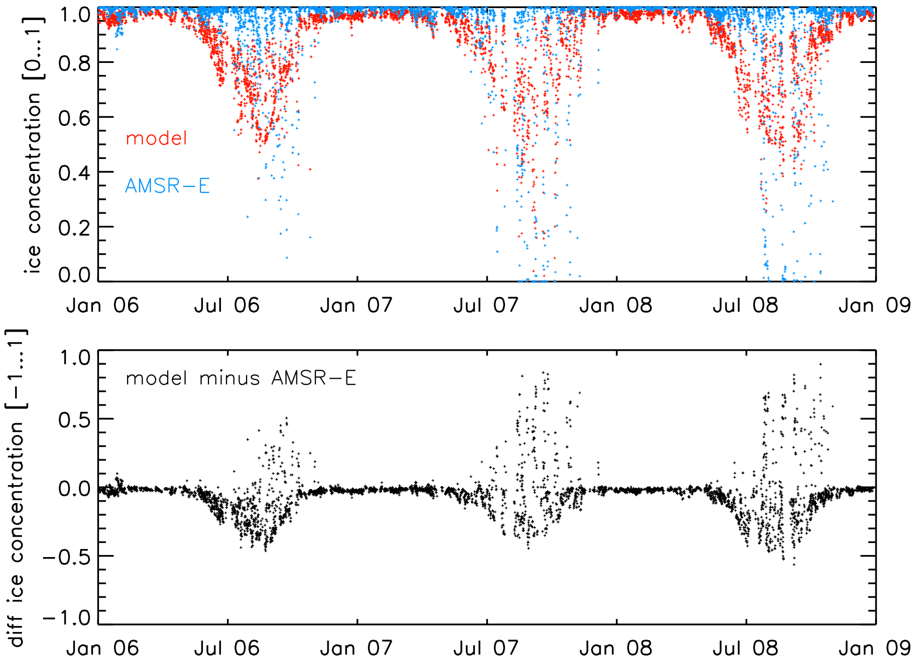

Fig. 2. Top: mean simulated and AMSR-E ice concentration within the cyclone radius for all 5057 detections. Bottom: difference between mean simulated and AMSR-E ice concentration.

TCD

7, 1141–1176, 2013

Cyclone impact on sea ice in the central Arctic Ocean

A. Kriegsmann and B. Brümmer

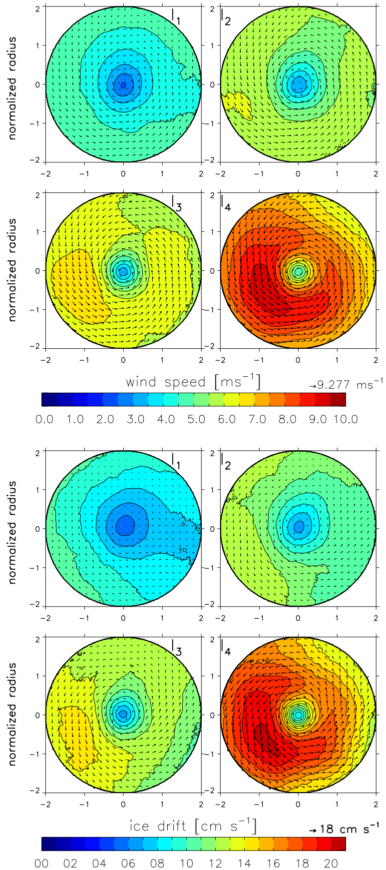

Fig. 3. Mean wind (top) and mean ice drift (bottom) for the intensity classes I_1 to I_4, centered on the location of the cyclone detection and normalized with the cyclone radius. Mean vectors as arrows, mean over absolute value of the speed as color.

TCD
7, 1141–1176, 2013

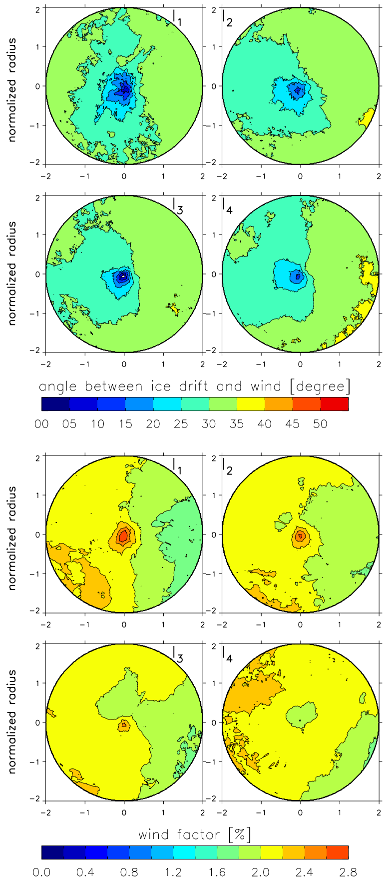

Fig. 4. Mean angle between wind forcing and ice drift (top) and mean wind factor (bottom) for the cyclone intensity classes I_1 to I_4.

TCD
7, 1141–1176, 2013

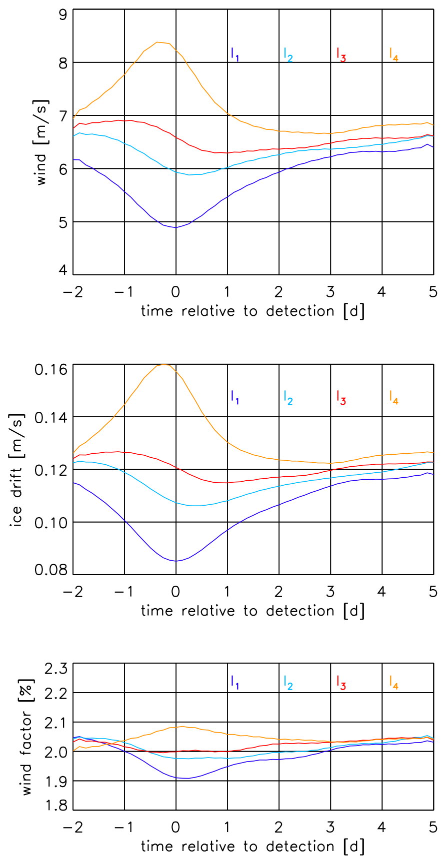

Fig. 5. Time series of wind (top), ice drift (middle), and wind factor (bottom) for different intensity classes. Shown are the mean values within the radius of the detections for the time period the two days before detection to five days after detection.

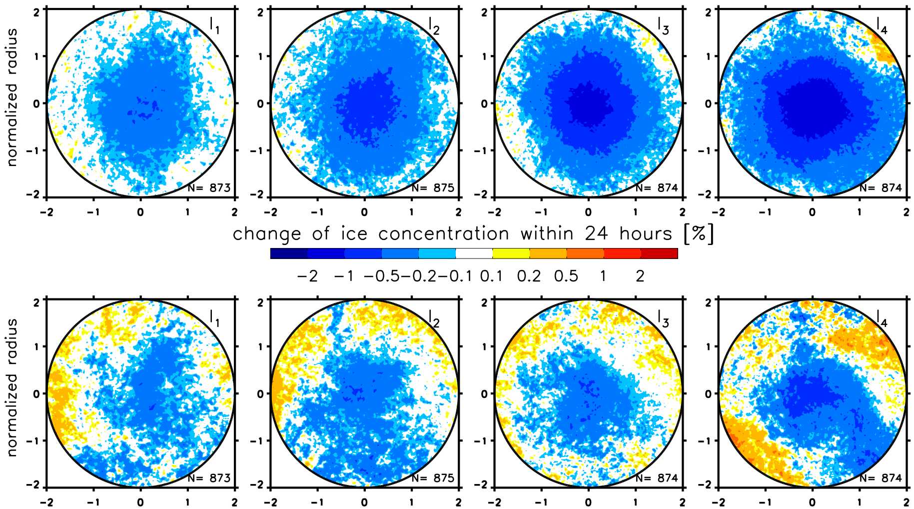

Fig. 6. Mean change of simulated (top) and AMSR-E (bottom) ice concentration within 24 h after cyclone detection for I_1 to I_4.

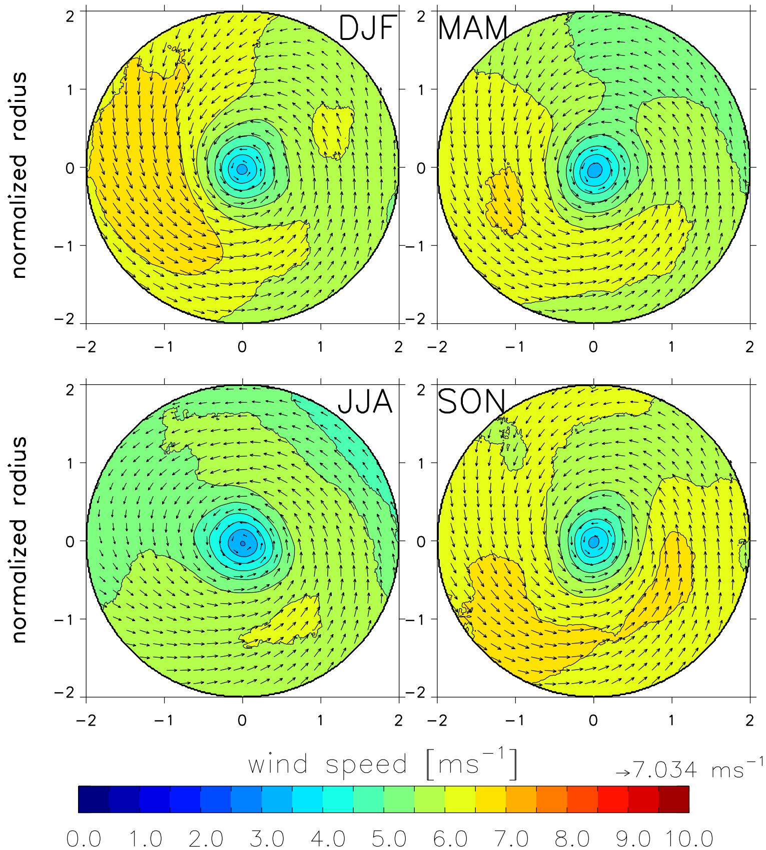

Fig. 7. Mean seasonal wind at the position of detection, normalized by radius. Shown are mean vector components and, as color, the mean value of wind speed.

TCD
7, 1141–1176, 2013

Cyclone impact on sea ice in the central Arctic Ocean

A. Kriegsmann and B. Brümmer

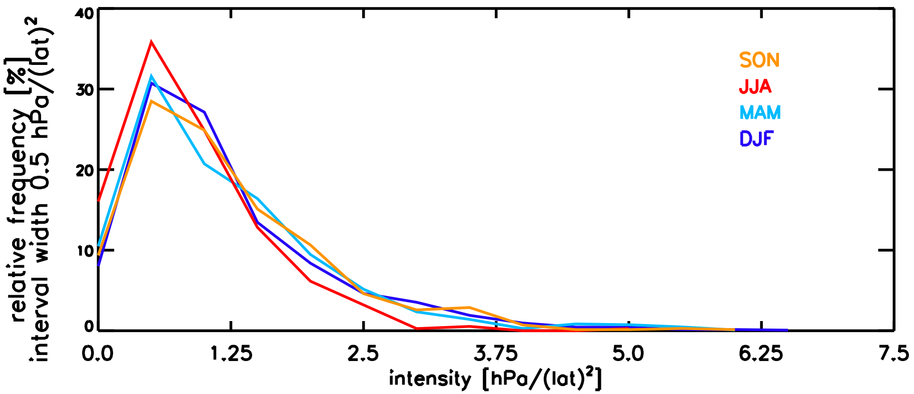

Fig. 8. Relative distribution of the intensity for the seasons.

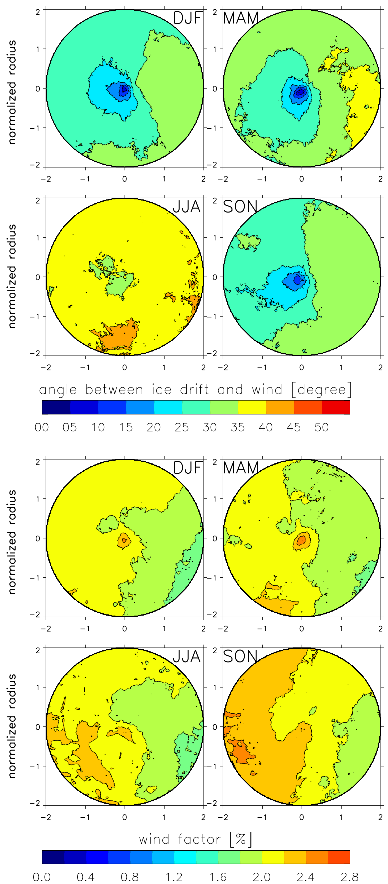

Fig. 9. Spatial distribution of the angle between wind forcing and ice drift (top) and the wind factor (bottom) for the different seasons.

TCD
7, 1141–1176, 2013

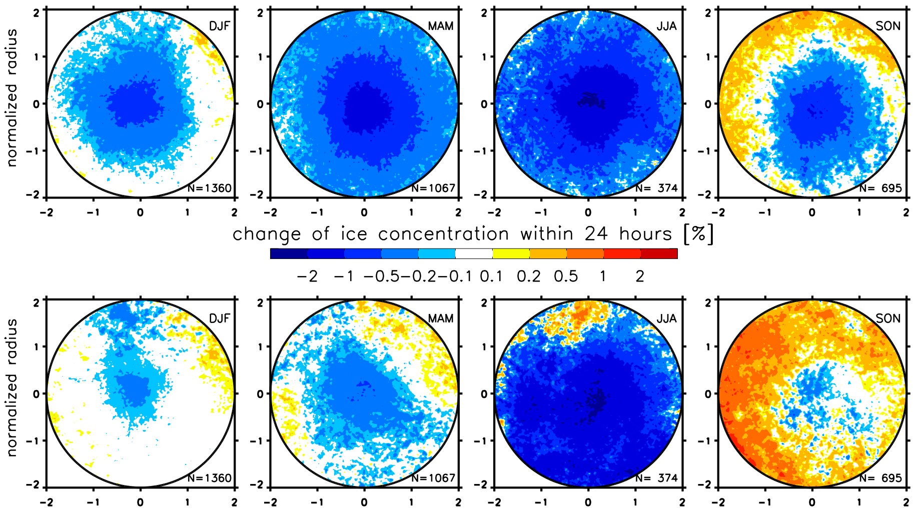

Fig. 10. Mean change of simulated (top) and AMSR-E (bottom) ice concentration within 24 h after cyclone detection fo each season.

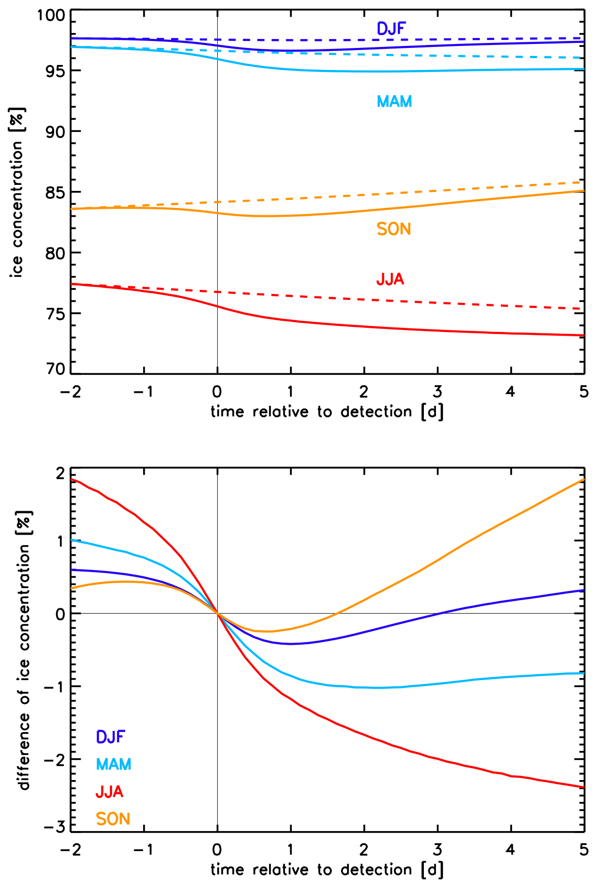

Fig. 11. Top: ice concentration in the period around the time of detection. As solid line: mean over all detections within the detection radius. As dashed line: ice concentration in the whole study area (shifted to the starting value of the corresponding solid line). Bottom: change in ice concentration, relatively to the time of detection.

TCD
7, 1141–1176, 2013

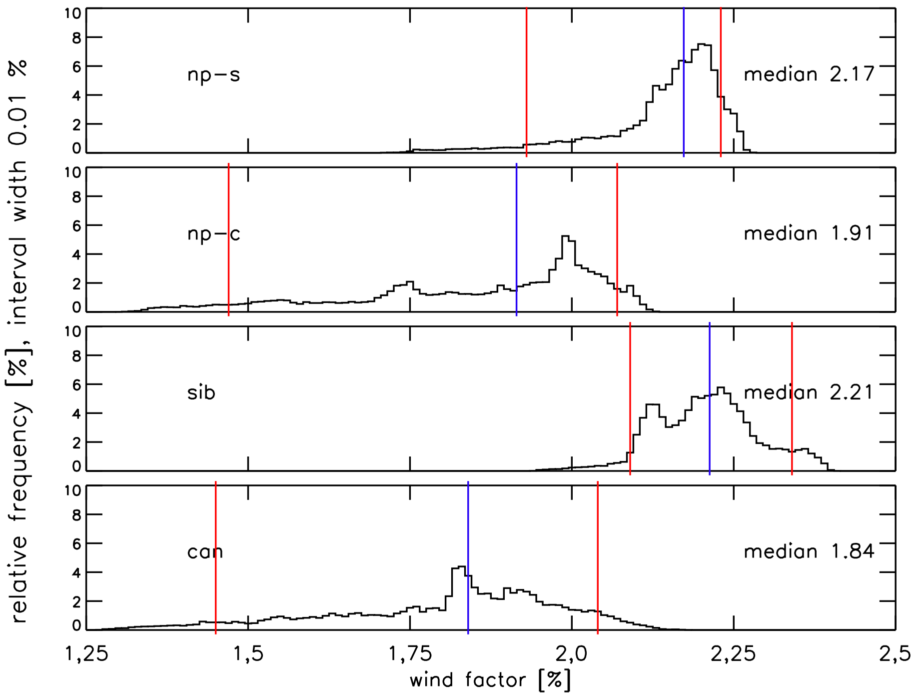

Fig. 12. Frequency distribution of the wind factor. Red lines mark the 5 %- and the 95 %-percentile, blue line the median.

TCD
7, 1141–1176, 2013

Cyclone impact on sea ice in the central Arctic Ocean

A. Kriegsmann and B. Brümmer

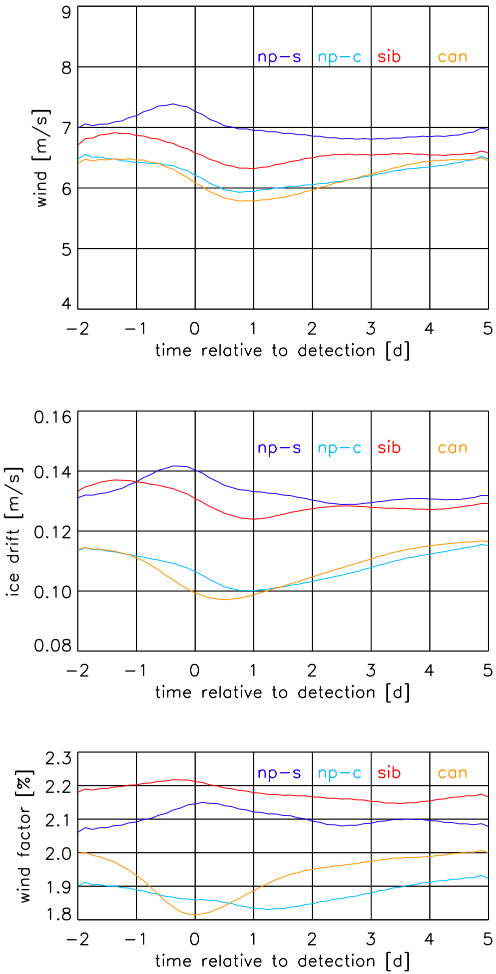

Fig. 13. As Fig. 5, but for the different regions.

TCD
7, 1141–1176, 2013

Cyclone impact on sea ice in the central Arctic Ocean

A. Kriegsmann and B. Brümmer

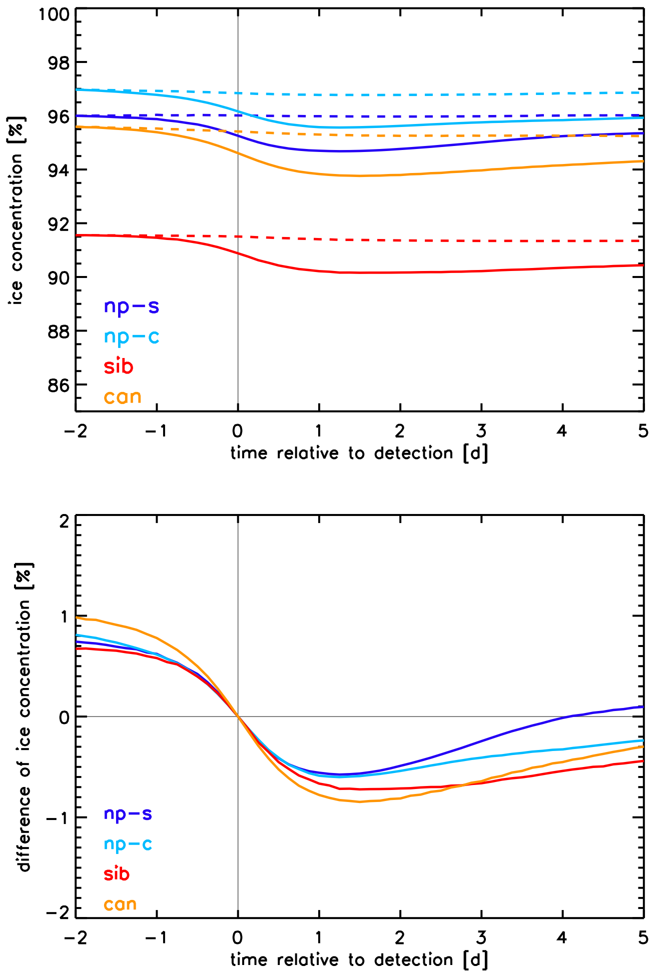

Fig. 14. As Fig. 11, but for the different regions.

TCD
7, 1141–1176, 2013

Cyclone impact on sea ice in the central Arctic Ocean

A. Kriegsmann and B. Brümmer